

# Experimental demonstration and modelling of an adsorption-enhanced reverse flow reactor for the catalytic combustion of coal mine ventilation air methane

Javier Fernández, Pablo Marín, Fernando V. Díez, Salvador Ordóñez\*

Department of Chemical and Environmental Engineering, University of Oviedo, Facultad de Química, Julián Clavería 8, Oviedo 33006, SPAIN

\* Phone: 34-985 103 437, FAX: 34-985 103 434, e-mail: [sordonez@uniovi.es](mailto:sordonez@uniovi.es)

## Abstract

Ventilation air methane is a major contributor to the carbon footprint of the coal mining industry. This contribution can be mitigated by combustion of methane to carbon dioxide. The use of efficient combustion devices, such as catalytic reverse flow reactors, can improve the economy of the process. However, the high water content of the ventilation air can inhibit catalysts (such as palladium) used in this process. To overcome this issue a novel reverse flow reactor with integrated separation, capable of adsorbing water from the feed before reaching the catalyst, is studied. The adsorbent is regenerated in situ thanks to the characteristic thermal pattern of reverse flow reactors. The application of this reactor design to the combustion of ventilation air methane has been demonstrated in a bench-scale device, operated at 0.15 m/s (n.t.p.) superficial velocity and different methane concentrations (1800-5400 ppm) and switching times (100-600 s). A mathematical model for this reactor has been proposed, the water adsorption parameters have been determined experimentally, and the model has been validated by comparison to bench-scale experimental results.

**Keywords:** adsorption, water inhibition, monolithic catalyst, regenerative catalytic oxidation, chromatographic reactor.

## Introduction

Environmental problems related to global warming have gained importance in the last decades. Coal mining is an activity with significant environmental impact. During coal extraction, important amounts of methane in air (concentration 0.1 to 1% vol.) are emitted to the atmosphere through the ventilation system (VAM, ventilation air methane). This emission is the main contribution (roughly 78%) to the carbon footprint of the coal mining activity [1].

In the atmosphere, methane is accumulated and eventually oxidized to carbon dioxide, but with a very slow kinetics. Methane average lifetime is around 12 years, and its effect as greenhouse gas is 23 times that of carbon dioxide (100 years-averaged Global Warming Potential). For this reason, combustion of methane to carbon dioxide before releasing to the atmosphere is of great environmental interest in order to reduce the net warming potential [2]. When the concentration of methane is high enough, part of the combustion heat can be recovered to produce steam or electricity, improving the economy of the process.

One suitable option for the oxidation of methane emitted in coal mining is the use of regenerative catalytic oxidation (RCO) in the so-called reverse flow reactors (RFR). This type of forced un-steady state reactor consists of a catalytic fixed bed in which the feed flow direction is periodically reversed. The selection of an appropriate flow reversal time (so called switching time) allows autothermal operation even for very lean methane concentrations. For moderate methane concentrations (more than 0.4%), it is also possible to recover a fraction of the heat released by the reaction. In this context, the catalyst has the advantage of reducing the ignition temperature of the methane/air mixture, increasing the thermal efficiency of the reactor and improving the efficiency of the heat recovery system. The typical reactor set-up consists of three beds: a catalytic bed in the center and two inert beds at both sides. At steady state, the feed stream enters the reactor at room temperature (20-30°C), is heated in the inert beds, and releases the heat of combustion in the catalytic bed (400-600°C) [3-4].

Coal mine ventilation air usually contains high amount of water (nearly at the saturation point), which is well-known to have a negative effect on the activity of combustion catalysts (particularly supported precious metals) [5,6]. In a previous work performed with coal mine emissions [7], it was found that the inhibition caused by water on a Pd-supported catalyst depends on water concentration and is reversible. Tests carried out in a bench-scale reverse flow reactor indicated that the stability of the reactor was negatively affected by water, and

increasing the reactor size was proposed to overcome the loss of catalyst activity caused by water [7]. However, this solution increases the investment and operation costs of commercial devices. For this reason, in the present work, a novel reverse flow reactor with integrated water separation, taking advantage of the flow reversal concept, is studied.

Several processes, such as reverse flow [8-10], loop [11-13] and chromatographic [14] reactors have been proposed for coupling reaction and separation by adsorption in forced unsteady state. Depending on the application, the compounds to be adsorbed are either reactants, products, catalyst inhibitors or the catalyst itself. Typically, these reactors can be used to prevent a reactant or product from leaving the reactor [15]. Moreover, these reactors have been found to be advantageous for the main reaction, increasing average reaction rates [16-18], shifting reaction equilibria [19], immobilizing homogeneous catalysts [20-21], or removing catalyst inhibitors [22]. For example, in the selective catalytic reduction of nitrogen oxides with ammonia, forced unsteady state reactors are used to increase the amount of ammonia adsorbed in the catalyst, and hence increase reaction rate [17, 23-24]. Another example, in the field of volatile organic compounds abatement, is the use of forced unsteady state reactors (reverse flow reactors, simulated moving bed reactors or reactor networks) to concentrate the organic compound prior to the oxidation [16,18,25-31]. The capture of the CO<sub>2</sub> generated by the reaction is also possible [15].

Bos et al. [22], proposed a reverse flow reactor design for VOC catalytic combustion, in which the material of the inert beds is totally or partially replaced by an adsorbent able to retain the water entering with the feed. This way, the inhibitory effect of water is avoided, because when the feed reaches the central catalytic bed, is free of water.

The adsorbent beds are not a mere guard bed, because the forced unsteady state character of RFR, together with its parabolic temperature profile (high temperature in the center and low temperature at the reactor sides), makes possible the self-regeneration of the adsorbent beds. Thus, in the first adsorbent bed (the first bed crossed by the feed when entering the RFR), water in the feed is adsorbed at low temperature (typically, the feed enters RFR at room temperature), and at the same time the feed temperature increases (because of the heat stored in the bed), so it reacts when reaches the central catalytic bed. The second adsorbent bed, placed after the catalytic bed, is at high temperature because the temperature plateau moves from the catalytic bed, causing the desorption of the water adsorbed in the previous cycle (TSA, temperature swing adsorption). Simultaneously, this bed stores the heat of

reaction. By inverting flow direction, the same process will happen in opposite adsorbent beds in the next cycle. The overall result is similar to water bypassing the central catalytic bed.

Bos et al. [22] demonstrated experimentally the working principle of this reactor design, by feeding air-water to a RFR with beds of zeolite as adsorbent. The bed was heated and the flow direction reversed to simulate a RFR. However, no catalyst was used or chemical reaction considered. They stated that more work was required for a more rigorous proof of the concept and the optimization of the reactor design and operation.

The aim of the present work is to experimentally demonstrate the validity of this concept (reverse flow combustor with integrated water adsorption), taking the catalytic combustion of ventilation air methane as case study. Due to the complexity of this reactor, in which many different phenomena take place, the use of mathematical models is needed for the optimization of design and operation. For this purpose, a phenomenological 1D heterogeneous dynamic model is formulated and validated with bench-scale experiments.

In order to accomplish these scopes, an appropriate adsorbent material, able to absorb water and at the same time act as thermal regenerator is firstly selected. Then, the application of the reverse flow reactor with integrated separation to the combustion of methane in presence of water is demonstrated in a bench-scale device. The influence of key variables such as methane and water concentrations and switching time is experimentally determined. After that, a mathematical model based on conservation equations for the entire process is formulated, considering both the reaction and adsorption zones. The adsorption equilibrium and mass transfer parameters, needed for the process modeling, are determined experimentally. Finally, the mathematical model is validated with the experiments.

## **Methodology**

### **Isothermal lab-scale adsorption experiments**

This reactor was used for adsorption experiments. The isothermal lab-scale reactor consisted of a stainless steel tube of 700 mm length and 9 mm diameter. The tube was filled with ground  $\gamma$ -alumina particles (500-710  $\mu\text{m}$ ), which were held in position with the help of a stainless steel mesh. The upstream part of the reactor was filled with 1 mm diameter glass spheres, used to help pre-heating the feed. The bed temperature, measured with a thermocouple introduced

inside the reactor tube, was regulated with a PID-controlled electric oven that surrounds the tube.

The reactor feed consisted of air from a compressor (Ingersoll-Rand). Flow rate (0.5 L/min n.t.p.) was set using a mass flow controller. Water was added to the air by bubbling through a flask equipped with a temperature-controller heating blanket. Depending on the temperature of the blanket and the water level inside the flask, a relative humidity of 20-80% (measured at 25°C) can be obtained (equivalent mole fraction of water 0.006-0.023). Water content of the reactor effluent was measured using a hygrometer (Vatsaia HMI 32).

### **Adiabatic bench-scale reactor**

The bench-scale reactor has been used to measure the rate of adsorption (mass transfer) and for the experimental demonstration of the reverse flow reactor with integrated separation applied to methane combustion in the presence of water.

The experimental device has been described in detail in previous works [25, 26, 28-31]. Here, only the basic information is provided. The reactor consisted of a 0.7 m long and 0.05 m internal diameter 316 stainless steel tube. This tube was filled with the RFR characteristic 3 bed layers: the catalytic bed in the middle (0.15 m long), formed by a commercial Pd-based monolith supplied by BASF (CPO-5M), and the heat storing-adsorbent beds (0.125 m long each) at both sides.

The catalytic monolithic block was formed by parallel channels with 390 cpsi cell density; this determines a cell size of 1 mm and a bed (or open) porosity of 65%. The channels are coated with a layer of washcoating with an average thickness of 81  $\mu\text{m}$  and accounting for 20% (vol.) of the solid. These geometrical properties have been determined experimentally with a stereomicroscope (Stemi 2000-C, ZEISS), as published elsewhere [7]. The solid density ( $\rho_s$ ), also measured experimentally, is 2300 kg/m<sup>3</sup>. Solid heat capacity ( $C_{ps}$ ) and thermal conductivity ( $k_s$ ), respectively 900 J/kg K and 0.8 W/m K, have been obtained from the literature for cordierite-based monoliths.

The temperature of the bed was measured in 5 points along the reactor axis using a multipoint thermocouple array. The reactor can be operated at nearly-adiabatic conditions with the help

of a multi-sectional electric oven, equipped with a dynamic temperature-control system able of compensating the heat transfer through the reactor wall [25, 26].

Reactor feed was prepared by mixing purified air from a compressor (Ingersoll-Rand) and a methane/air synthetic mixture (2.5% vol.) from a cylinder (Air Liquide) in adequate proportions. The flow rate was controlled using two mass flowmeters (Bronkhorst F201C); total flow rate was fixed to 15 L/min (n.t.p.). Water was introduced into the system using a bubbling flask equipped with a temperature-controlled heating blanket. A relative humidity of 60-95% (measured at 25°C, equivalent mole fraction of 0.017-0.027) was obtained using this device.

The water content of the reactor effluent was measured using a hygrometer (Vatsaia HMI 32). Methane concentration was analyzed on-line using an infrared spectrometer (ABB URAS14). Water was eliminated from the gas stream at the spectrometer inlet using a bed of silica, in order to avoid interferences in the measurements.

### **Reverse flow reactor model**

Mathematical models, when validated with experimental data, are very useful tools in the design, optimization and operation of commercial reactors. In this work the reverse-flow reactor with integrated separation was simulated with a phenomenological model obtained from mass and energy conservation equations. Based on the previous experience with forced unsteady state reactors, a 1D heterogeneous dynamic model has been found to be a good choice [3, 25, 28-30]. The model predicts the dynamic evolution of temperature and concentration along the reactor beds. Property gradients are expected only in the axial direction, because the reverse flow reactor will operate at adiabatic conditions. Heterogeneous models, where conservation equations are applied separately to the gas and solid phases, predict the accumulation of heat and mass in the solid with higher accuracy, which is of great importance for reverse flow reactors with integrated separation.

The conservation equations corresponding to the model are shown in Table 1. These equations have been solved using Danckwerts boundary conditions. The meaning of the symbols is indicated in the list of symbols. The mass balances, formulated for methane and water, are valid for both the catalyst and adsorbent beds, but with different physical and transport properties in each case. For the methane balance, there is no accumulation in the solid

( $\partial n_i / \partial t = 0$ ), so the partial differential equation is simplified into an algebraic equation. For the case of water, an expression for the adsorption equilibrium is required to relate concentrations in the solid ( $n_i$ ) and at the gas-solid interphase ( $c_{Si}$ ). This expression was determined experimentally, as explained later.

Reaction rate for methane combustion on a Pd-based monolithic catalyst is given by a Langmuir-Hinshelwood equation that takes into account inhibition caused by water, obtained experimentally in a previous work [7]:

$$-r_{CH_4} = \frac{k_w p_{CH_4}}{1 + K_{inh} p_{H_2O}} \quad (1)$$

Where  $p_{CH_4}$  and  $p_{H_2O}$  are methane and water partial pressures, respectively, and  $k_w$  and  $K_{inh}$  are temperature-dependent parameters ( $R = 8.314 \text{ J mol}^{-1} \text{ K}^{-1}$ ):

$$k_w = 1.56 e^{-80000/RT} \text{ mol kg}_{cat}^{-1} \text{ s}^{-1} \text{ Pa}^{-1} \quad (2)$$

$$K_{H_2O} = 8.07 \cdot 10^{-9} e^{67600/RT} \text{ Pa}^{-1} \quad (3)$$

This rate law was developed in the absence of mass and heat transfer resistances (e.g. using ground catalyst). When applied for a monolithic catalyst, an effectiveness factor is used to account for the mass transfer resistance in the washcoating layer. This effectiveness factor is calculated using Thiele modulus and the textural properties of the catalyst [7]. The expressions are summarized in Table 2.

Transport properties, such as mass and heat gas-to-solid transfer coefficients and axial effective dispersion coefficients, are calculated using correlations from the literature, adequate for the type of bed (monolith or random particles), as indicated in a previous work [29, 31] and summarized in Table 2. The geometrical and physical properties of the beds are indicated in the following sections. Gas density is calculated using ideal gas law.

This mathematical model has been solved by means of the ‘method of lines’, where the spatial derivatives are approximated by finite differences obtained from Taylor polynomials. The resulting set of ordinary differential equations is solved using MATLAB (function *ode15s*). The

switching of the feed direction is modeled by shifting the boundary conditions. This method has been proved to be accurate in previous works [29, 30].

## Results and discussion

### Selection of the adsorbent

In our reverse flow reactor with integrated separation, the adsorbent packed in the two non-catalytic beds must trap water from the gaseous feed during the first semi-cycle, and adsorbed water must be desorbed in the second semi-cycle, so good adsorption capacity at inlet conditions (low temperature), and ability to desorb water at the conditions during the reverse cycle (130-350°C) are required. Moreover, as the adsorbent replaces (at least partially) the inert bed in which heat is stored and released, good thermal properties are also desirable.

Typical water adsorbents are  $\gamma$ -alumina, silica and molecular sieves (zeolites).  $\gamma$ -Alumina is the cheapest one, but usually exhibits the lowest adsorption capacity. Regarding thermal properties, the most important for reverse flow reactors is thermal inertia (product of density and heat capacity,  $\rho_s C_{ps}$ ). Thus, a material with high thermal inertia is able to store more energy, reducing the size of the reactor [31]. Thermal inertia of  $\gamma$ -alumina, silica and molecular sieves are 530, 200 and 200 kJ/m<sup>3</sup> °C, respectively [32]. Taking into account these properties,  $\gamma$ -alumina was initially selected for our reactor.

So, the adsorbent used was a commercial  $\gamma$ -alumina supplied by BASF in the form of cylindrical pellets (4 mm diameter). The equivalent diameter (sphere of equal surface to volume ratio) was calculated as 5.6 mm. This adsorbent is a mesoporous material with 7.1 nm BJH average pore size and 242 m<sup>2</sup>/g BET surface area, both properties measured by nitrogen physisorption. The density of the adsorbent, 1060 kg/m<sup>3</sup>, and the bed porosity, 40%, were also measured experimentally. The heat capacity (836 J/kg K) and the thermal conductivity (0.5 W/m K) were taken from the literature [32].

The regeneration capability of  $\gamma$ -alumina has been studied in a temperature programmed desorption (TPD) experiment. The sample initially saturated with water at 20°C was heated in a helium flow at 3°C/min. The water desorbed from the sample was measured on-line using a mass spectrometer. The experiment indicated that water desorption starts at 100°C and by 200°C 83% of the water had desorbed. This temperature matches the temperature of the inert

bed during the desorption cycle in the reverse flow reactor with integrated separation (130-350°C), so according to these results  $\gamma$ -alumina is a good choice.

### **Demonstration experiments**

In this section, the operation of reverse flow reactors with integrated adsorption for combustion of organic compounds in humid air is tested by reacting methane in the adiabatic bench-scale RFR with integrated adsorption described previously. The total gas flow rate (measured at normal conditions) was 15 L/min (n.t.p.), which corresponds to a superficial velocity in the reactor of 0.15 m/s (n.t.p.). The feed was introduced in the reactor, initially pre-heated, at room temperature (20°C) with methane concentration in the range 1800-5400 ppm. Water molar fraction was kept in the range 0.021 to 0.024, and reactor switching time was varied within the range 100-600 s.

Figure 1 shows the temperature profiles obtained at the middle of cycle number 15 for two experiments (3600 ppm methane and switching times 100 and 300 s, respectively). In the same plots, the equivalent experiments carried out in the reactor without adsorbent and in the absence of water have also been depicted. As it has been explained, water produces an inhibitory effect on the catalyst, reducing the reaction rate. Thus, methane conversion decreases, resulting in a decrease in bed temperature, as observed when the experiment without adsorbent is compared to the experiment with no water. This effect reduces the stability of the reactor, as will be discussed later. On the other hand, the reverse flow reactor with water and integrated adsorption exhibits a temperature profile very close to the corresponding to the absence of water. This indicates that a similar amount of heat is being released by the reaction and hence the reaction is taking place at a similar reaction rate, and suggests that the adsorbent is trapping the water and preventing catalyst inhibition. These experiments demonstrate in a practical application and at bench-scale that the concept of the reverse flow reactor with integrated adsorption can be successfully implemented.

Figure 1 gives also information on the effect of switching time. Thus, at low switching time the high temperature plateau in the center of the reactor is wider and at higher temperature, which is beneficial for the stability of the reactor. On the contrary, at high switching times the heat wave moves within the reactor bed in a wider extension. As a consequence, less heat is trapped inside the reactor and hence the reactor stability decreases. Switching time affects the

reactor in the same way with and without adsorbent. However, as switching time is also the regeneration time of the adsorbent (time during which water desorbs from the beds), some discrepancies might be observed if the adsorbent is not fully regenerated at the end of the cycle, e.g. using very small switching times.

All the experiments carried out in the reverse flow reactor with integrated adsorption are analyzed in terms of stability using the switching time versus concentration plot in Figure 2. Stable operation means that the reactor reaches an oscillating pseudo-steady state that can be maintained indefinitely. For comparison purposes, the stability regions determined in a previous work [7] without adsorbent, in the presence (dotted line) and absence (dashed line) of water are also depicted. Stable operation is attained for combinations of feed methane concentration and switching time above the lines. The presence of water with no adsorbent reduces the stability of the reactor (range of variables that lead to stable operation). This can be overcome by increasing methane concentration, decreasing the switching time (to some extent) or increasing the reactor size. It can be clearly observed that within the experimental range considered, the stability of the reactor with water adsorption is similar to the reactor when no external water is added to the feed.

### **Adsorption equilibrium**

The mathematical model of the reverse flow reactor with integrated adsorption requires the modeling of the water adsorption process. Experimental measurements of the adsorption of water in  $\gamma$ -alumina have been done in the isothermal fixed-bed reactor described in the methodology section. The reactor was filled with 1 g of ground  $\gamma$ -alumina particles (500-710  $\mu\text{m}$ ). This size was found small enough to consider negligible mass transfer resistances, as indicated below.

Experiments have been done using the step-response method, in which a step of water concentration in air is imposed over a previously desorbed alumina sample (by heating at 300°C). Figure 3 shows, as an example, the breakthrough curve obtained at 44.5°C and 0.022 water mole fraction. The influence of the piping and the hygrometer on the response dynamics has been evaluated by means of blank tests at the same conditions, but in the absence of adsorbent, and the inherent breakthrough adsorption curves have been obtained by deconvolution of the blank tests, as shown in Figure 3. Thus, the dynamic response inherent to

the adsorbent is a step response, indicating the absence of axial dispersion in the bed (plug flow) and mass transfer resistances, and instantaneous adsorption.

Breakthrough curves were determined for four temperatures (44-120°C) and four water mole fractions (0.010-0.030). In all the cases, the inherent response of the adsorbent was a step response.

The adsorption capacity of the adsorbent at the equilibrium ( $n_i^*$ ) was calculated from the breakthrough curves by means of a mass balance:

$$n_i^* = \frac{F_{i0} \theta_{ads}}{W} \quad (4)$$

Where  $\theta_{ads}$  is the ideal breakthrough time of the deconvoluted response. The results obtained at different operating conditions are depicted in Figure 4.

Experimental adsorption equilibrium results were first modeled according to the Langmuir isotherm, but the results were not satisfactory. Best results were obtained using the Freundlich isotherm:

$$n_i^* = K_i c_i^m \quad (5)$$

Where the adsorption equilibrium constant is considered to follow van't Hoff equation,  $K_i = K_{i,ref} e^{-(\Delta H_{ads}/R)(1/T-1/T_{ref})}$ .

The model parameters were fitted to the experimental data by the non-linear least-square method using MATLAB software (function *lsqcurvefit*). The exponent of Freundlich model was found to be  $m = 0.5 \pm 0.1$ , the enthalpy of adsorption  $\Delta H_{ads} = -25 \pm 2$  kJ/mol and  $K_{i,ref} = 2.5 \pm 0.3$  m<sup>1.5</sup> kg<sup>-1</sup> mol<sup>0.5</sup> at  $T_{ref} = 373$  K.

The quality of the fitting can be evaluated in Figure 4. Overall, the model predicts well the experimental data.

## Mass transfer in the adsorption sections

In the previous section, the adsorption equilibrium was determined in absence of mass transfer resistances (using ground adsorbent). The aim of this section is to characterize the water mass transfer from the gas to the solid adsorbent when in form of pellets, as used in the RFR with integrated adsorption, so that water mass transfer can be incorporated to the reactor mathematical model. For this purpose, the bench-scale fixed-bed reactor described in the methodology section has been used.

The step-response method is applied to a bed formed by a commercial adsorbent in the form of cylindrical pellets (diameter 4 mm). The length of the bed was 0.25 m (adsorbent weight 310 g), equivalent to the total inert bed length used in the experiments with the reverse flow reactor. The methodology is based on applying step changes in the feed water concentration (mole fraction 0.029), while the rest of variables are maintained constant, as described in the previous section. The tests have been done at isothermal conditions using a multi-section electric oven surrounding the reactor tube. Before the experiment, the bed was heated above 300°C to desorb all the water.

Figure 5 (symbols) shows the adsorption breakthrough curves obtained at different temperatures (28-163°C) and 15 L/min (n.t.p.) flow rate, which corresponds to 0.15 m/s (n.t.p.) superficial velocity. These curves are inherent breakthrough curves, since the dynamics of the piping and hygrometer have been accounted for by means of blank tests. It can be observed that on increasing temperature, the adsorption capacity of the bed decreases (lower break time), as a consequence of the displacement of the adsorption equilibrium. The sigmoidal shape of the curves indicates the existence of important mass transfer resistance, deviations from plug flow, or both effects.

The Peclet number,  $Pe = u_0 L / \epsilon_b D_{ax}$ , accounts for deviations from the ideal plug flow pattern (plug flow  $Pe = \infty$  and perfect mixing  $Pe = 0$ ).  $Pe$  has been calculated for the operating conditions of this work using the correlation for random packings proposed by Edwards and Richardson [33]. The value obtained,  $Pe = 140-150$ , which indicates small deviations from plug flow, so the sigmoidal shape of the breakthrough curves can be attributed to mass transfer.

The adsorption of water in a fixed bed consisting of commercial  $\gamma$ -alumina particles is modeled by the conservation equations in Table 1. The bed is considered isothermal, so only the mass

balances to water, with no reaction ( $r_i = 0$ ), are considered. The balances are written in dimensionless form taking into account the following definitions:  $x_i = c_i/c_{i0}$ ,  $w_i = n_i/n_{i0}^*$ ,  $\tau = t/\theta_{ads}$  and  $\xi = z/L$ .

$$\frac{1}{\Lambda} \frac{\partial x_i}{\partial \tau} = -\frac{\partial x_i}{\partial \xi} + \frac{1}{Pe} \frac{\partial^2 x_i}{\partial \xi^2} - Da (x_i - x_{si}) \quad (6)$$

$$\frac{\partial w_i}{\partial \tau} = Da (x_i - x_{si}) \quad (7)$$

Where  $\theta_{ads} = n_{i0}^* W/F_{i0}$  is the ideal break time (eq. 4),  $n_{i0}^* = K_i c_{i0}^m$  is the solid concentration in equilibrium with the feed concentration ( $c_{i0}$ ),  $Pe = u_0 L/\epsilon_b D_{ax}$  is the Peclet number,  $Da = aK_C W c_{i0}/F_{i0} \rho_S (1 - \epsilon_b)$  is the Damköhler number and  $\Lambda = n_{i0}^* \rho_S (1 - \epsilon_b)/c_{i0} \epsilon_b$  is the dimensionless adsorption capacity.

These partial differential equations are coupled by the equilibrium model (Freundlich isotherm): in dimensionless form,  $x_{si} = w_i^{1/m}$  with  $m = 0.5$ . The system of equations has been solved with MATLAB (function *pdepe*) using Danckwerts boundary conditions.

The dimensionless form of the equations only contains four parameters ( $\Lambda$ ,  $Pe$ ,  $Da$  and  $m$ ). As indicated previously, axial mixing can be neglected, so  $Pe$  is not considered. The Damköhler number ( $Da$ ) and the dimensionless adsorption capacity ( $\Lambda$ ) have been calculated by non-linear least-square fitting to the breakthrough curves obtained at the different operating conditions:  $Da = 510, 240, 140$  and  $100 \pm 40$ ;  $\Lambda = 18\,200, 15\,690, 13\,370$  and  $12\,350 \pm 30$ ; respectively, for 28, 75, 114 and 163°C. Model predictions in Figure 5 show that the model predicts well both break times and the shape of the curves.

The fitted parameters,  $Da$  and  $\Lambda$ , have been used to calculate the gas to solid global mass transfer coefficient of water,  $aK_C$ , and the water adsorption equilibrium constant,  $K_i$ , needed for the RFR modeling. Both properties are temperature-dependent.

The mass transfer coefficient is known to depend on temperature following a power-law expression,  $aK_c = aK_{c,T_{ref}}(T/T_{ref})^n$ . This equation has been fitted to the values of  $aK_c$  calculated at different temperatures. The fitting parameters, calculated by least-square regression, are  $aK_{c,T_{ref}} = 210 \pm 20 \text{ s}^{-1}$  and  $n = -3.6 \pm 0.8$ , with  $T_{ref} = 373 \text{ K}$ . Figure 6a shows that the model is adequate in the temperature range considered. The regression coefficient is  $R^2 = 0.98$ .

The same procedure has been followed for the adsorption equilibrium constant. The adsorption equilibrium constant follows an exponential dependence with temperature, the so-called van't Hoff equation,  $K_i = K_{i,ref} e^{-(\Delta H_{ads}/R)(1/T - 1/T_{ref})}$ . The linear representation of this equation is depicted in Figure 6b for the fitted parameters  $K_{i,ref} = 5.2 \pm 0.5 \text{ m}^{1.5} \text{ kg}^{-1} \text{ mol}^{0.5}$  and  $\Delta H_{ads} = -4.7 \pm 1.2 \text{ kJ/mol}$ , with  $T_{ref} = 100^\circ\text{C}$ . The regression coefficient is  $R^2 = 0.993$ .

### Model validation

In this section, the proposed mathematical model (based on conservation equations) for the reverse flow reactor with integrated adsorption, including the models for water adsorption equilibrium and mass transfer developed in the previous chapter, is used to simulate the reverse flow reactor with integrated adsorption. The capability of the model is evaluated by comparison of model predictions to the experiments. No model parameter has been adjusted in this stage.

Results obtained in the experiments performed at different operating conditions are shown in Figures 7 to 9. Comparison is done in terms of the evolution of the temperature profiles, found to be a good method in previous works with reverse flow reactors [29-31]. Thus, temperature is measured directly in the experiments and the values and shape of the curves depend on the interrelation of many key phenomenological properties, such as thermal capacity, heat transport rate, reaction rate, etc. Since temperature profiles in the reverse flow reactor are symmetrical, only the evolution of temperature in three reactor positions are depicted. Overall, the model is able to produce good predictions.

Next, the performance of the model is discussed in more detail. Figure 7 corresponds to the experiment at 3600 ppm methane and 300 s switching time. These conditions lead to stable operation, but are close to the limit of instability (Figure 2). The model predicts the oscillations

of temperature caused by the periodic change in the flow direction, and the greatest discrepancies are observed in the middle of the bed.

When decreasing switching time to 100 s, Figure 8, temperature increases at the beginning of the test due to the accumulation of heat. After some cycles, temperature decreases to the pseudo-steady state value, resulting in stable reactor operation. On the contrary, when the concentration of methane is decreased to 1800 ppm (switching time 300 s), Figure 9, the reactor is unstable and temperature decreases progressively towards extinction. The model is capable of predicting also the temperature evolution in this unstable experiment.

According to these results, the mathematical model proposed for the reverse flow reactor with integrated adsorption can be considered as validated. Since this model has been validated at adiabatic conditions, the scale-up to industrial scale reactors (which are commonly adiabatic) is straightforward, and hence the model can be used in the design and optimization of this type of reactors.

## Conclusions

Water present in coal mine ventilation air produces important inhibition on palladium-based combustion catalysts. This results in loss of efficiency in catalytic reverse flow reactors used to combust the ventilation air methane. In the present work, the reverse flow reactor with integrated water separation by adsorption, used for combusting methane in presence of water, has been experimentally tested and modeled.

The reverse flow reactor used was a bench-scale unit, provided with catalytic bed (Pd containing commercial monolith) and  $\gamma$ -alumina adsorbing beds, and able of operating at nearly adiabatic conditions. Experiments in this device showed that the adsorbent is able to separating the water from the feed, eliminating catalyst inhibition. Moreover, the adsorbent is regenerated in situ at a higher temperature during the reverse cycles of the reactor, so that the reactor operation is efficient and stable.

A 1D heterogeneous dynamic model based on mass and energy conservation equations has been developed for the reactor, including water adsorption equilibrium, that was found to fit the Freundlich isotherm, and the adsorption related mass transfer processes, that were found to be kinetically relevant. This reactor model was used for simulating all the bench-scale experiments. The model predicts well the behavior of the reverse flow reactor with integrated

adsorption, so it can be considered validated to be used in the design and optimization of such devices.

## Acknowledgements

This work was supported by the Research Fund for Coal and Steel of the European Union (contract UE-10-RFCR-CT-2010-00004), and by the Asturian Government (contract GRUPIN14-078). The catalyst was gratefully provided by BASF.

## Nomenclature

$a$	solid surface to bed volume ratio ( $\text{m}^2/\text{m}^3$ )
$c_i$	molar concentration ( $\text{mol}/\text{m}^3$ )
$C_p$	heat capacity ( $\text{J}/\text{kg K}$ )
$D_{ax}$	axial dispersion coefficient ( $\text{m}^2/\text{s}$ )
$Da$	Damköhler number (-)
$D_{ep}$	effective diffusion coefficient in the porous catalyst ( $\text{m}^2/\text{s}$ )
$D_h$	hydraulic diameter of the monolith (m)
$d_p$	particle diameter (m)
$E_a$	activation energy ( $\text{kJ}/\text{mol}$ )
$F_i$	molar flow rate ( $\text{mol}/\text{s}$ )
$f_w$	fraction of washcoating (% vol.)
$h$	gas to solid heat transfer coefficient ( $\text{W}/\text{m}^2 \text{K}$ )
$K_C$	gas to solid mass transfer coefficient ( $\text{m}/\text{s}$ )
$k_g$	thermal conductivity of the gas ( $\text{W}/\text{m K}$ )
$K_{inh}$	Freundlich equilibrium constant ( $(\text{mol}/\text{kg}_{\text{ads}})/(\text{mol}/\text{m}^3)^m$ )
$k_w$	kinetic constant ( $\text{mol}/\text{kg}_{\text{cat}} \text{s Pa}$ )
$L_w$	washcoat thickness (m)
$m$	Freundlich exponent
$n_i$	concentration of adsorbed species in the solid ( $\text{mol}/\text{kg}$ )
$un$	Nusselt number
$p_i$	partial pressure (Pa)
$Pe$	Peclet number (-)

<b>Pr</b>	Prandlt number (-)
$r_i$	reaction rate (mol/kg <sub>cat</sub> s)
<b>R</b>	ideal gas law constant (8.314 J/mol K)
<b>Re</b>	Reynold number (-)
<b>Sc</b>	Schmidt number (-)
<b>Sh</b>	Sherwood number (-)
<b>t</b>	time (s)
<b>T</b>	temperature (K)
$t_{sw}$	switching time (s)
<b>u</b>	gas superficial velocity (m/s)
<b>v</b>	gas interstitial velocity (m/s)
<b>W</b>	weight (kg)
$w_i$	dimensionless adsorbed concentration (-)
$x_i$	dimensionless gas concentration (-)
<b>y</b>	mole fraction (-)
<b>z</b>	spatial coordinate (m)

#### Greek symbols

$\epsilon_b$	bed porosity (-)
$\Delta H_i$	enthalpy of reaction (J/mol)
$\phi$	Thiele modulus (-)
$\kappa_{ax}$	axial thermal conductivity (W/m K)
$\eta$	catalyst internal effectiveness factor (-)
$\Lambda$	dimensionless adsorption capacity (-)
$\theta_{ads}$	ideal break time (s)
$\rho$	density (kg/m <sup>3</sup> )
$\xi$	dimensionless bed length (-)
$\tau$	dimensionless time (-)

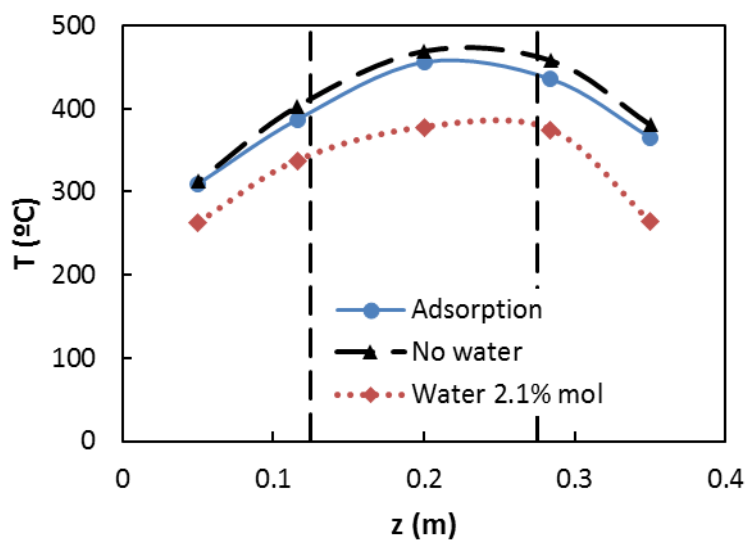
#### Subscripts

0	inlet
cat	catalyst
G	gas
ref	reference
S	solid

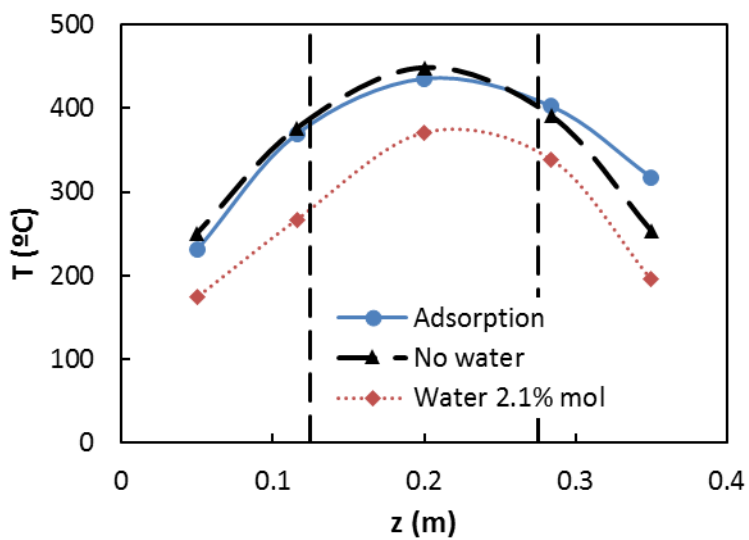
## Caption to figures

- Figure 1 Performance of the RFR with integrated adsorption (●): temperature profiles at the middle of cycle 15. Comparison to equivalent experiments in the absence of water (▲) and with no adsorbent (◆).  
a).  $y_{G0} = 3600$  ppm,  $t_{sw} = 100$  s.  
b).  $y_{G0} = 3600$  ppm,  $t_{sw} = 300$  s.
- Figure 2 Summary of the experiments with the RFR with integrated adsorption: stable (●) and unstable (○) operation. Stability limits with no adsorbent: with water in the feed (⋯), no water in the feed (— —).
- Figure 3 Adsorption breakthrough curve at 44.5°C and 0.022 water mole fraction: (⋯) blank measurement, (—) adsorption measurement and (—) deconvoluted signal.
- Figure 4 Equilibrium adsorption capacity at different operating conditions (symbols) and Freundlich isotherm predictions (lines). Temperature: (◆) 44°C, (●) 60°C, (■) 80°C, (▲) 120°C.
- Figure 5 Adsorption breakthrough curves obtained in the presence of mass transfer resistance. Symbols: experiments. Lines: model fitting. Surface velocity 0.15 m/s (n.t.p.). Step of water mole fraction 0.029. Temperature: (▲) 28°C, (●) 75°C, (◆) 114°C, (■) 163°C.
- Figure 6 a) Adjustment of the global mass transfer coefficient.  
b) Adjustment of the Freundlich constant.  $T_{ref} = 373$  K
- Figure 7 Validation of the mathematical model for the RFR with integrated adsorption. Evolution of temperature at different catalytic bed positions: experiments (—) and simulations (—).  $y_{G0} = 3600$  ppm,  $t_{sw} = 300$  s.
- Figure 8 Validation of the mathematical model for the RFR with integrated adsorption. Evolution of the temperature at different catalytic bed positions: experiments (—) and simulations (—).  $y_{G0} = 3600$  ppm,  $t_{sw} = 100$  s.
- Figure 9 Validation of the mathematical model for the RFR with integrated adsorption. Evolution of the temperature at different catalytic bed positions: experiments (—) and simulations (—).  $y_{G0} = 1800$  ppm,  $t_{sw} = 100$  s.

Figure 1



(a)



(b)

Figure 2

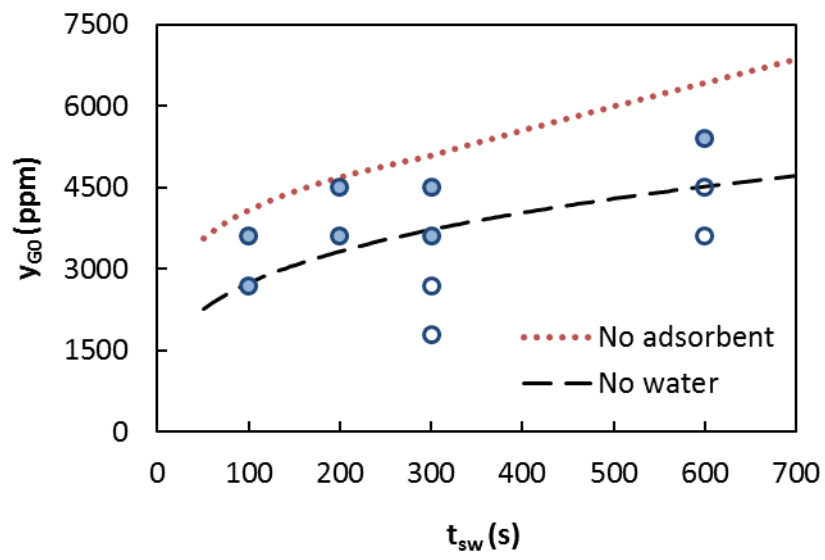


Figure 3

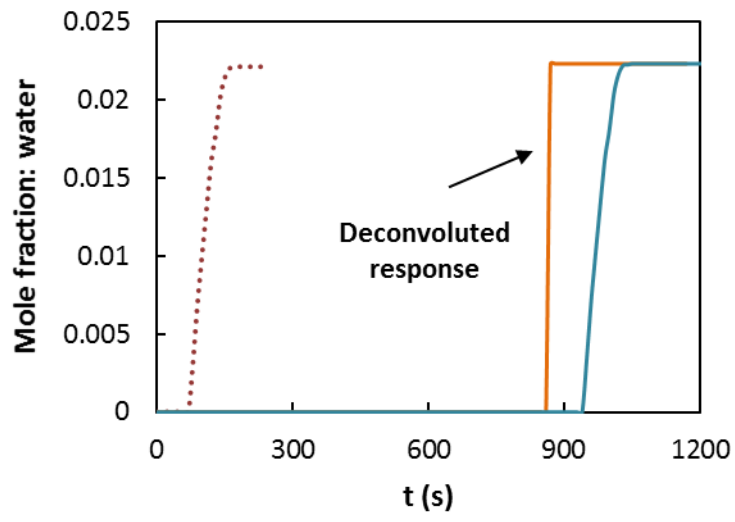


Figure 4

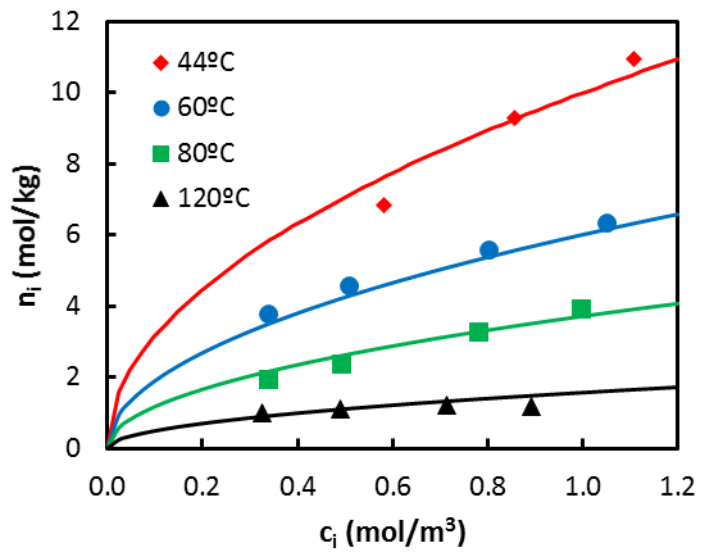


Figure 5

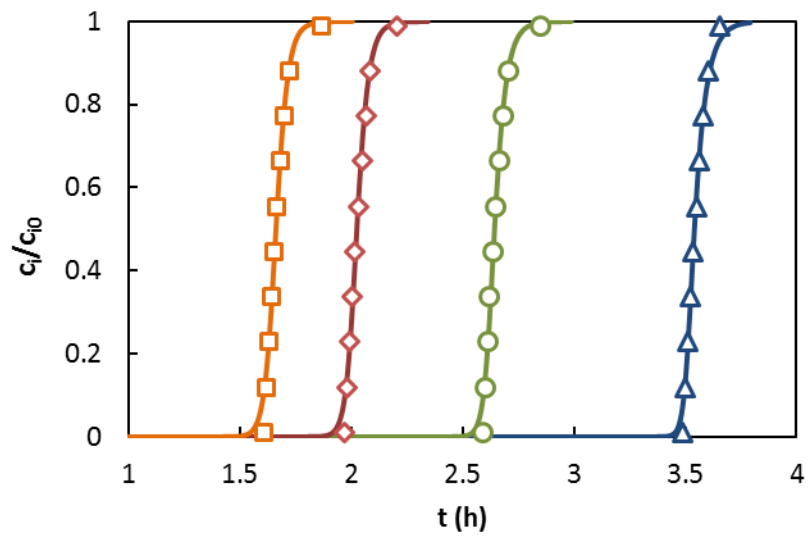
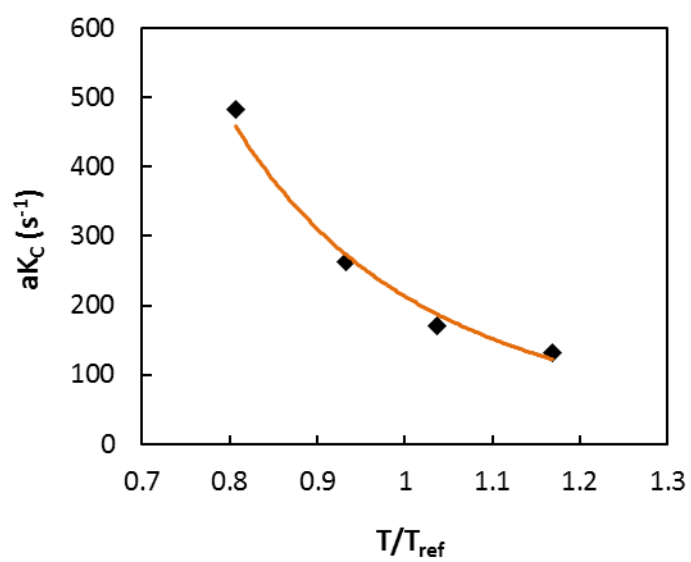
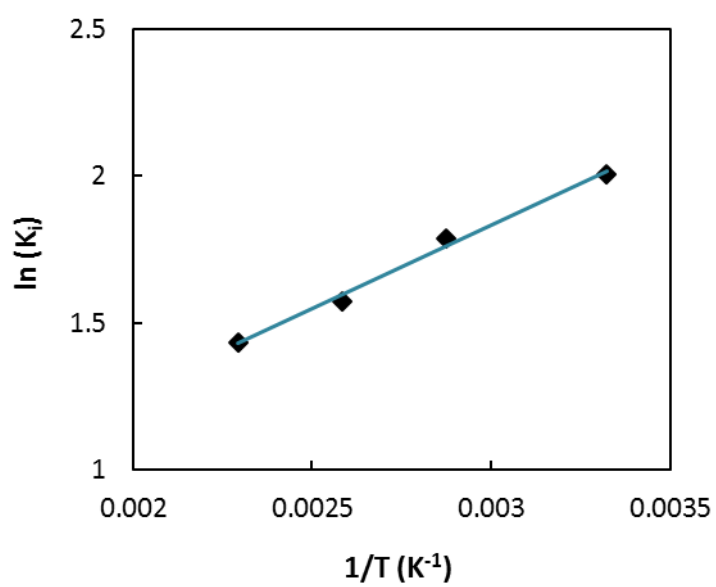


Figure 6



(a)



(b)

Figure 7

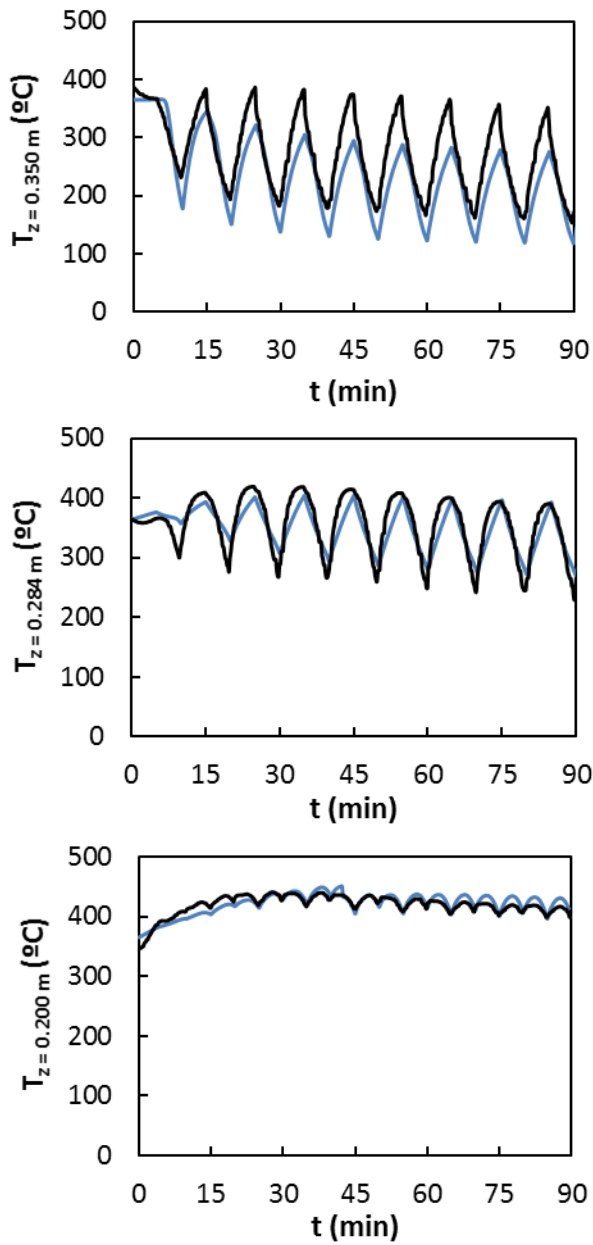


Figure 8

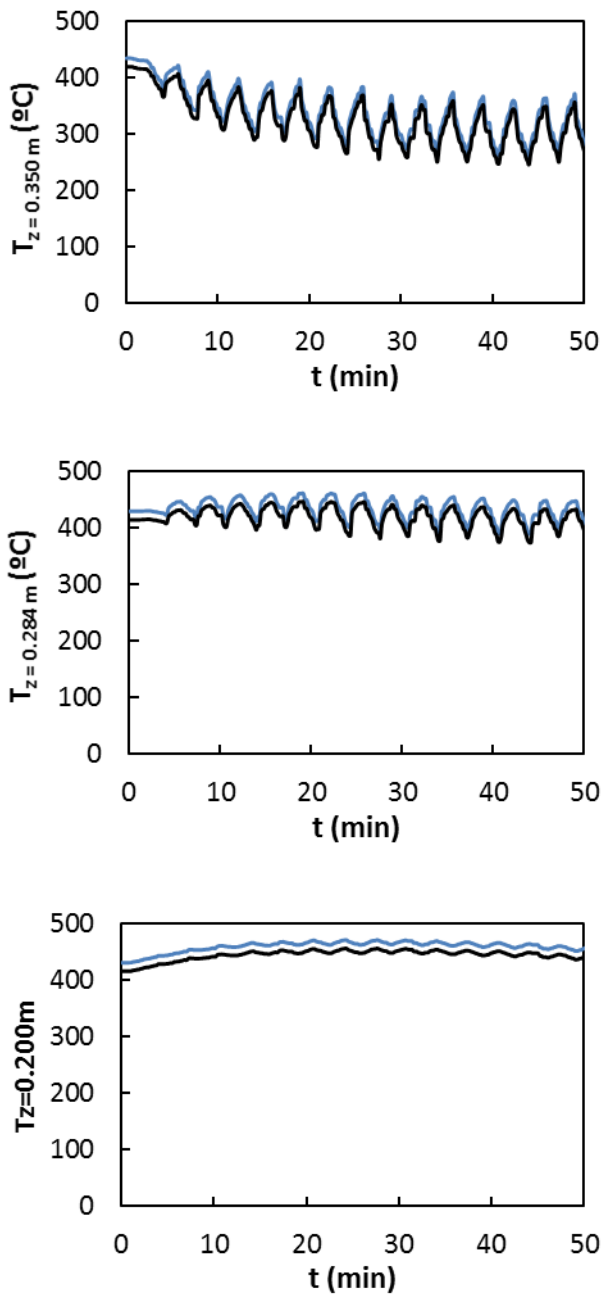
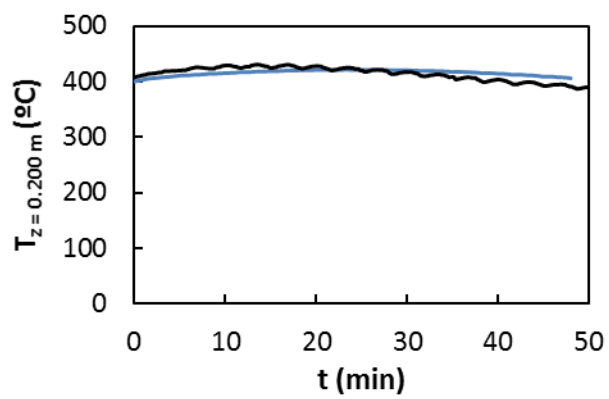
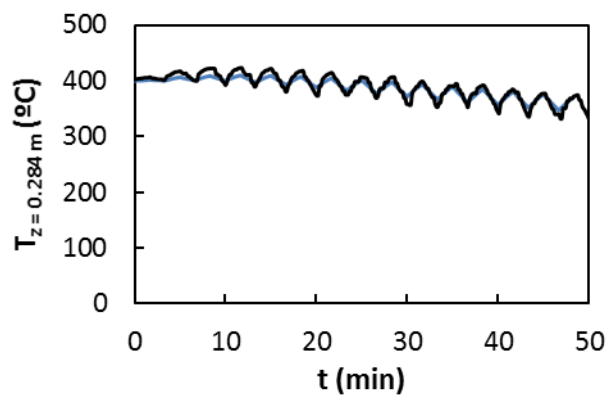
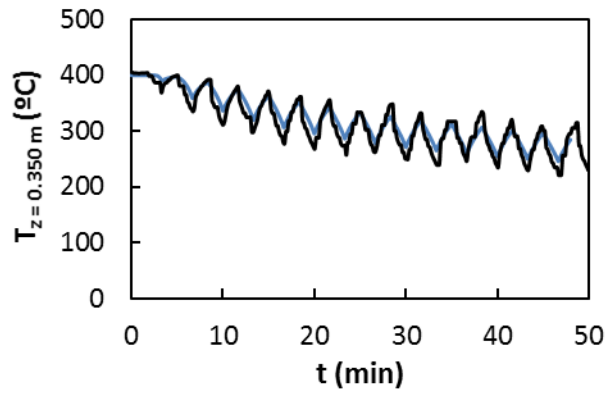


Figure 9



## List of tables

Table 1 Conservation equations for the reverse flow reactor with integrated adsorption: heterogeneous 1D dynamic model.

Mass balances
$\frac{\partial c_i}{\partial t} = -\frac{u_0}{\epsilon_b} \frac{\rho_{G0}}{\rho_G} \frac{\partial c_i}{\partial z} + D_{ax} \frac{\partial^2 c_i}{\partial z^2} - \frac{aK_C}{\epsilon_b} (c_i - c_{Si})$
$\frac{\partial n_i}{\partial t} = \frac{aK_C}{\rho_S(1 - \epsilon_b)} (c_i - c_{Si}) + \eta r_i$
Energy balances
$\frac{\partial T_G}{\partial t} = -\frac{u_0}{\epsilon_b} \frac{\rho_{G0}}{\rho_G} \frac{\partial T_G}{\partial z} + \frac{\kappa_{Gax}}{\rho_G C_{PG}} \frac{\partial^2 T_G}{\partial z^2} + \frac{ah}{\rho_G C_{PG} \epsilon_b} (T_S - T_G)$
$\frac{\partial T_S}{\partial t} = \frac{\kappa_{Sax}}{\rho_S C_{PS}} \frac{\partial^2 T_S}{\partial z^2} + \frac{ah}{\rho_S C_{PS} (1 - \epsilon_b)} (T_G - T_S) + \frac{\rho_{cat} \eta r_i \Delta H_i}{\rho_S C_{PS}}$

Table 2 Expressions used to calculate physical, chemical and transport properties.

<b>Catalytic bed</b>	
Kinetic equation (methane)	$r_{CH_4} = -\frac{k_w p_{CH_4}}{1 + K_{inh} p_{H_2O}} = -k'_w p_{CH_4}$ $k_w = 1.56 e^{-80000/RT_S} \text{ mol}/(\text{kg}_{\text{monolith}} \text{ s Pa})$ $K_{inh} = 8.07 \cdot 10^{-9} e^{67600/RT_S} \text{ Pa}^{-1}$
Effectiveness factor (methane)	$\eta = \frac{\tanh \phi}{\phi}, \quad \phi = L_w \sqrt{\frac{k'_w \rho_{cat} RT_S}{f_w D_{\epsilon p}}}$
Surface to volume ratio of the bed	$a = (4/D_h) \epsilon_b$
Mass transfer (methane)	$K_C = (D_{im}/D_h) \text{Sh}, \quad \text{Sh} = 2.977 \text{ (laminar)}$
Heat transfer	$h = (k_g/D_h) \text{Nu}, \quad \text{Nu} = 2.977 \text{ (laminar)}$
Axial dispersion (mass)	$D_{ax} = D_h v \left[ \frac{1}{\text{Re Sc}} + \frac{\text{Re Sc}}{192} \right]$
Axial dispersion (energy)	$\kappa_{G,ax} = D_h v \rho_G C_{PG} \left[ \frac{1}{\text{Re Pr}} + \frac{\text{Re Pr}}{192} \right]$
<b>Adsorbent bed</b>	
Adsorption equilibrium (water)	$n_i^* = K_{eqi} c_i^m \rightarrow c_{Si} = (n_i/K_{eqi})^{1/m}, \quad m = 0.5$ $K_{eqi} = 1.14 e^{4700/RT_S} \text{ (mol/kg}_{\text{ads}})(\text{m}^3/\text{mol})^{0.5}$
Surface to volume ratio of the bed	$a = (6/d_p)(1 - \epsilon_b)$
Global mass transfer (water)	$aK_C = 210 (T_S/373)^{-3.6} \text{ s}^{-1}$
Heat transfer	$h = (k_g/d_p) \text{Nu}, \quad \text{Nu} = 2 + \text{Re}^{1/2} \text{Pr}^{1/3}$
Axial dispersion (mass)	$D_{ax} = d_p v \left[ \frac{0.73}{\text{Re Sc}} + \frac{0.5}{1 + \frac{9.7}{\text{Re Sc}}} \right]$
Axial dispersion (energy)	$\kappa_{G,ax} = d_p v \rho_G C_{PG} \left[ \frac{0.73}{\text{Re Pr}} + \frac{0.5}{1 + \frac{9.7}{\text{Re Pr}}} \right]$

$$R = 8.314 \text{ J/mol K}$$



## References

- [1] E. Díaz, J. Fernández, S. Ordóñez, N. Canto, A. González, Carbon and ecological footprints as tools for evaluating the environmental impact of coal mine ventilation air, *Ecological Indicators* 18 (2012) 126-130.
- [2] I. Karakurt, G. Aydin, K. Aydiner, Mine ventilation air methane as a sustainable energy source, *Renewable and Sustainable Energy Reviews* 15 (2011) 1042-1049.
- [3] G. Eigenberger, G. Kolios, U. Nieken, Thermal pattern formation and process intensification in chemical reaction engineering, *Chemical Engineering Science* 62 (2007) 4825-4841.
- [4] Y.S. Matros, G.A. Bunimovich, Reverse-Flow operation in fixed bed catalytic reactors, *Catalysis Reviews* 38 (1996) 1 - 68.
- [5] D. Ciuparu, L. Pfefferle, Support and water effects on palladium based methane combustion catalysts, *Applied Catalysis A: General* 209 (2001) 415-428.
- [6] P. Hurtado, S. Ordóñez, H. Sastre, F.V. Díez, Combustion of methane over palladium catalysts in the presence of inorganic compounds: inhibition and deactivation phenomena, *Applied Catalysis B: Environmental* 47 (2004) 85-93.
- [7] J. Fernández, P. Marin, F.V. Díez, S. Ordóñez, Coal mine ventilation air methane combustion in a catalytic reverse flow reactor: Influence of emission humidity, *Fuel Processing Technology* 133 (2015) 202-209.
- [8] I. Yongsunthon, E. Alpay, Design of periodic adsorptive reactors for the optimal integration of reaction, separation and heat exchange, *Chemical Engineering Science* 54 (1999) 2647-2657.
- [9] A.A. Barresi, G. Baldi, D. Fissore, Forced unsteady-state reactors as efficient devices for integrated processes: Case histories and new perspectives, *Industrial & Engineering Chemistry Research* 46 (2007) 8693-8700.
- [10] M. Cittadini, M. Vanni, A.A. Barresi, Transient behaviour and start-up of periodic flow reversal reactors for catalytic decontamination of waste gases, *Chemical Engineering and Processing* 41 (2002) 437-443.
- [11] M. Brinkmann, A.A. Barresi, M. Vanni, G. Baldi, Unsteady state treatment of very lean waste gases in a network of catalytic burners, *Catalysis Today* 47 (1999) 263-277.
- [12] D. Fissore, A.A. Barresi, Comparison between the reverse-flow reactor and a network of reactors for the oxidation of lean VOC mixtures, *Chemical Engineering & Technology* 25 (2002) 421-426.
- [13] M.A.G. Hevia, D. Fissore, S. Ordóñez, F.V. Díez, A.A. Barresi, Combustion of medium concentration CH<sub>4</sub>-air mixtures in non-stationary reactors, *Chemical Engineering Journal* 131 (2007) 343-349.
- [14] H.S. Caram, G.A. Viecco, Analysis of the reverse flow chromatographic reactor, *AIChE Journal* 50 (2004) 2266-2275.
- [15] A.Y. Madai, M. Sheintuch, Reduction in greenhouse gases emission in a loop reactor adsorber: Simulations and experiments, *Chemical Engineering Science* 65 (2010) 5392-5401.
- [16] M.A. Kolade, A. Kogelbauer, E. Alpay, Adsorptive reactor technology for VOC abatement, *Chemical Engineering Science* 64 (2009) 1167-1177.

- [17] E. Muñoz, P. Marín, F.V. Díez, S. Ordóñez, Selective catalytic reduction of NO in a reverse-flow reactor: Modelling and experimental validation, *Applied Energy* 138 (2015) 183-192.
- [18] Y. Zhang, E. Doroodchi, B. Moghtaderi, Chemical looping combustion of ultra low concentration of methane with Fe<sub>2</sub>O<sub>3</sub>/Al<sub>2</sub>O<sub>3</sub> and CuO/SiO<sub>2</sub>, *Applied Energy* 113 (2014) 1916-1923.
- [19] G.A. Viecco, H.S. Caram, Comparison between simulated moving bed and reverse flow chromatographic reactors for equilibrium limited reactions, *Chemical Engineering Science* 61 (2006) 6869-6879.
- [20] J. Dunnewijk, H. Bosch, A.B. de Haan, Reverse flow adsorption: integrating the recovery and recycling of homogeneous catalysts, *Separation and Purification Technology* 40 (2004) 317-320.
- [21] K.G.W. Hung, D. Papadias, P. Bjornbom, M. Anderlund, B. Akermark, Reverse-flow operation for application of imperfectly immobilized catalysts, *Aiche Journal* 49 (2003) 151-167.
- [22] A.N.R. Bos, J.P. Lange, G. Kabra, A novel reverse flow reactor with integrated separation, *Chemical Engineering Science* 62 (2007) 5661-5662.
- [23] D. Fissore, A.A. Barresi, C.C. Botar-Jid, NO<sub>x</sub> removal in forced unsteady-state chromatographic reactors, *Chemical Engineering Science* 61 (2006) 3409-3414.
- [24] D. Fissore, O.M. Penciu, A.A. Barresi, SCR of NO<sub>x</sub> in loop reactors: Asymptotic model and bifurcational analysis, *Chemical Engineering Journal* 122 (2006) 175-182.
- [25] D. Fissore, A.A. Barresi, G. Baldi, M.A.G. Hevia, S. Ordóñez, F.V. Díez, Design and testing of small-scale unsteady-state afterburners and reactors, *AIChE Journal* 51 (2005) 1654-1664.
- [26] M.A.G. Hevia, S. Ordóñez, F.V. Díez, D. Fissore, A.A. Barresi, Design and testing of a control system for reverse-flow catalytic afterburners, *AIChE Journal* 51 (2005) 3020-3027.
- [27] Y.O. Jeong, D. Luss, Pollutant destruction in a reverse-flow chromatographic reactor, *Chemical Engineering Science* 58 (2003) 1095-1102.
- [28] P. Marín, S. Ordóñez, F.V. Díez, Monoliths as suitable catalysts for reverse-flow combustors: modelling and experimental validation, *AIChE Journal* 56 (2010) 3162-3173.
- [29] C.R. Thompson, P. Marín, F.V. Díez, S. Ordóñez, Evaluation of the use of ceramic foams as catalyst supports for reverse-flow combustors, *Chemical Engineering Journal* 221 (2013) 44-54.
- [30] P. Marín, M.A.G. Hevia, S. Ordóñez, F.V. Díez, Combustion of methane lean mixtures in reverse flow reactors: Comparison between packed and structured catalyst beds, *Catalysis Today* 105 (2005) 701-708.
- [31] D. Fissore, A.A. Barresi, On the influence of the catalyst physical properties on the stability of forced unsteady-state after-burners, *Chemical Engineering Research & Design* 81 (2003) 611-617.
- [32] D.W. Green, R.H. Perry, *Perry's Chemical Engineers' Handbook*, 8th ed., McGraw-Hill 2008.
- [33] M.F. Edwards, J.F. Richardson, Gas dispersion in packed beds, *Chemical Engineering Science* 23 (1968) 109-123.